

## MI RF Cavity Tuning Control System Characterization

3/1/2007

T.Berenc, S.Kotz

**Introduction:** The Main Injector cavity tuning control system has been characterized to guide future upgrade designs. The relationship between the ferrite tuner biasing current and the cavity resonant frequency has been measured as well as the dynamic response due to Eddy current effects in the tuners. The complete system response has been modeled to first order and included in a time-varying state space simulation and compared to test station measurements.

### Principle of Present Cavity Tuning Control Scheme

The present cavity tuning control scheme is based upon the simple fact that in a parallel RLC circuit the phase angle between the generator current and the circuit voltage is zero when the circuit resonance is tuned to the drive frequency. Figure 1 shows a simplified block diagram of a typical MI cavity tuning control system for a ferrite tuned cavity driven by both an RF power tube and a beam image current. The power tube is cathode driven with the tube anode current,  $I_G$ , being directly proportional to the cathode voltage to first order. Thus, by detecting the phase between the tube anode voltage and the cathode voltage, one can effectively measure the load angle presented to the power tube. By controlling the DC biasing field in the ferrite tuners, the effective inductance of the cavity impedance is changed; thus controlling the cavity resonant frequency.

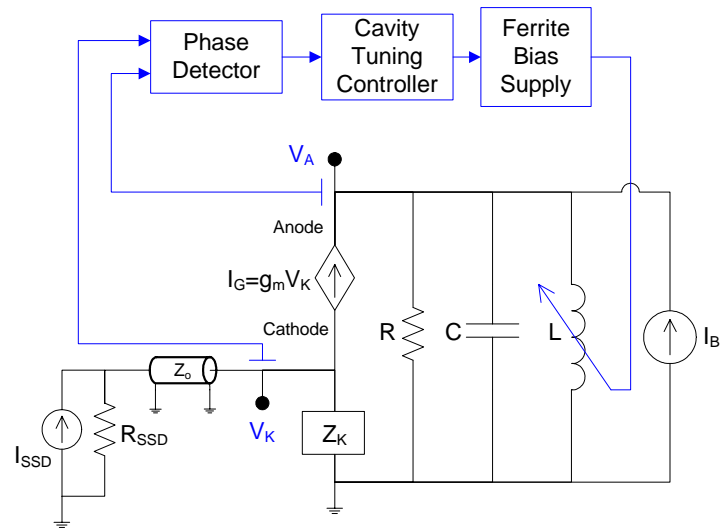


**Figure 1:** Typical cavity tuning control scheme block diagram.

This discussion uses the terminology conventions of Ref. [1] and [2] in which the circuit phasor diagram is referenced to the cavity (anode) voltage lying on the horizontal axis and the generator load angle,  $\phi_L$ , is defined as the phase of the generator current relative to the cavity voltage. It is a simple detail but careful attention has to be made with regards to the definition of the relative phase angles.

The equations from [1] and [2] relevant to this discussion are summarized here for convenience:

The cavity impedance is expressed as:

$$Z(f) = R \cos \phi_Z e^{j\phi_Z} \quad (1) \quad \text{with} \quad \tan \phi_Z = Q \left( \frac{f_o^2 - f^2}{f \cdot f_o} \right) \cong 2Q \frac{\Delta f}{f_o} \quad (2) \quad \text{and} \quad \Delta f \equiv f_o - f \quad (3)$$

where:

- $f$  : is the drive frequency of the generator current
- $f_o$  : is the cavity resonant frequency
- $R$  : is the shunt impedance (including the tube output impedance for this discussion)
- $Q$  : is the quality factor  $Q = 2\pi f_o RC$  (loaded Q for this discussion)
- $\phi_Z$  : is the impedance phase angle

From the circuit phasor diagram [2], the cavity (anode) voltage phasor  $\hat{V}_A$  is expressed as:

$$\hat{V}_A = \hat{I}_T \cdot Z \quad (4) \quad \text{where} \quad \hat{I}_T = \hat{I}_G + \hat{I}_B = \frac{I_o}{\cos \phi_Z} e^{-j\phi_Z} \quad (5)$$

where:

- $\hat{I}_G = I_G e^{j\phi_L}$  : is the generator (tube) current phasor
- $\hat{I}_B = I_B e^{-/(+)j\left[\frac{\pi}{2} + \phi_S\right]}$  : is the beam image current phasor (transformed to the anode) with the -/(+) sign used for below/(above) transition
- $I_o \equiv \frac{|V_A|}{R}$  : is the current necessary to generate  $|V_A|$  with no detuning ( $\phi_Z = 0$ ).

The generator current magnitude,  $I_G$ , and load angle,  $\phi_L$ , are expressed via:

$$I_G = \frac{I_o (1 + Y \sin \phi_S)}{\cos \phi_L} \quad (6) \quad \text{and} \quad \tan \phi_L = \frac{-\tan \phi_Z + /(-)Y \cos \phi_S}{(1 + Y \sin \phi_S)} \quad (7)$$

where:

- $\phi_S$  : is the beam synchronous phase angle
- +/(-) : indicates below/(above) transition in (7)
- $Y \equiv \frac{I_B}{I_o}$  : is the beam loading factor

An important feature of Eq.(6) is revealed for **steady-state** conditions: that the generator current is minimized if  $\phi_L = 0$  (the tube sees a real impedance). The emphasis is on *steady-state* since the peak generator power can be reduced in transient conditions (beam gaps) if *half-detuning* is used [3].

The present MI cavity tuning control system classically regulates the load angle  $\phi_L$  to zero. Not only does this minimize the generator current in steady-state conditions, but it also fortunately satisfies the low intensity Robinson stability criterion [4] ( $f_o > f$  below transition and  $f_o < f$  above transition). This is seen by setting  $\phi_L = 0$  in Eq. (7) resulting in  $\tan \phi_Z = +/(-)Y \cos \phi_S$ . Even in the presence of beam gaps, the control scheme tends towards this condition since it is really an averaged value of  $\phi_L$  that the controller works on. This was shown in [5] during which the detuning was shown to go through the half-detuning condition during the multi-batch loading of the MI.

In the absence of beam loading,  $Y = 0$ , Eq. (7) shows that  $\phi_L = -\phi_Z$ ; thus allowing for a direct measurement of the cavity detuning angle,  $\phi_Z$ , from the  $\phi_L$  phase detector. If beam gaps are long enough, the natural transients of the system will have decayed between beam pulses to allow a direct measurement of the detuning angle. Unfortunately, the longest beam gap in the multi-batch slip-stacking scheme proposed for the Proton Plan is only 1/14 of the MI ring when the machine is fully loaded; only ~0.8usec. The lowest effective quality factor of a MI cavity impedance with 15dB of direct RF feedback is  $\sim 3000/(1+6)$  or  $\sim 430$ . This corresponds to a voltage decay time of  $\tau_E = 2 Q_{eff} / \omega = \sim 2.6$  usec. Thus the ~0.8usec gap is not sufficiently long enough to allow for the cavity detuning angle to be directly measured during the beam gaps.

## Cavity Detuning Measurement Tool

A simple cavity detuning measurement tool was developed during the Proton Plan power measurement studies as briefly mentioned in Ref.[5]. Further details are documented here:

As discussed above, in the absence of beam loading,  $\phi_L = -\phi_Z$ . If the cavity tuning control system has been calibrated such that  $\phi_L = -\phi_Z = 0$  without beam loading, then the relationship between the cavity resonant frequency and the Ferrite Bias Supply (FBS) current,  $I_{FBS}$ , can be measured during no beam conditions. Under these conditions, it can be assumed that the cavity resonant frequency,  $f_o$ , is equal to the low-level RF (LLRF) drive frequency,  $f$ .  $I_{FBS}$  and  $f$  can be monitored via ACNET parameters I:FBxxI and I:VFOUT respectively; where xx is the MI RF station number 01 to 18 of interest. Thus a cavity tuning measurement tool does the following:

- (1) During a no-beam cycle two time functions are measured via ACNET:  $I_{FBS}(t)$  and  $f(t)$ .
- (2) The tool interpolates each function to a common time base,  $t_C$ , since ACNET parameters do not necessarily share a common time stamp and forms a sampled dataset of  $(f(t_C), I_{FBS}(t_C))$  values.

- (3) A function  $f_o(I_{FBS})$  fitting this dataset is found. A 3<sup>rd</sup> order polynomial fit is used in W20. An exponential function shows more promise for extrapolation purposes. The details of the functional fit are discussed in a separate section below.
- (4)  $f^{beam}(t)$  and  $I_{FBS}^{beam}(t)$  are then measured as the RF drive frequency and the FBS current during beam conditions. (again a common time base is used)
- (5) Using  $f_o(I_{FBS})$ , the cavity resonant frequency with beam is calculated as  $f_o(t) = f_o(I_{FBS}^{beam}(t))$
- (6) The detuning angle,  $\phi_z(t)$ , is calculated using Eq. (2) with Q approximated via the linear function  $Q(f_o(t)) = 6835.27 \cdot f_o(t) - 357980.2$  where it is assumed that the cavity Q is 3000 at injection frequency (52.8114 MHz) and 5000 at extraction (53.104 MHz).

An example detuning measurement from [5] is shown in Fig. 2 and 3 for a ‘non slip-stacking’ station (a station that is held ‘off’ during the slip-stacking process) during a typical MI mixed-mode cycle (2 batches slip-stacked for pBar production plus 5 batches for NuMI).

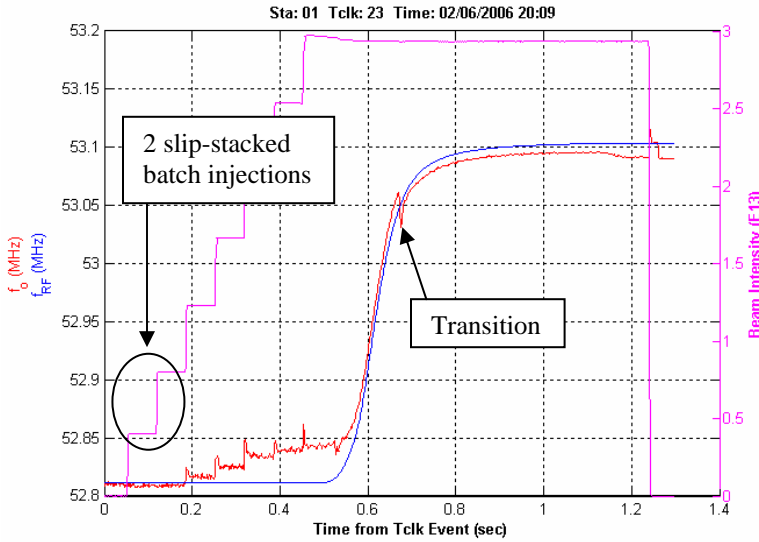


**Figure 2:** Example measurement results of  $f_o$  and  $f$  during a typical MI mixed-mode cycle (2 batches being slip-stacked for pBar production + 5 batches for NuMI).

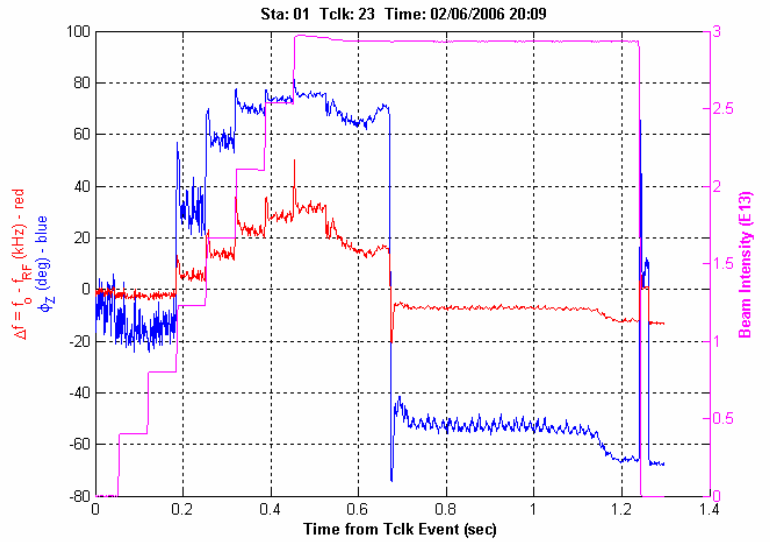


**Figure 3:** Example  $\Delta f$  and  $\phi_z$  calculations for Fig. 2.

There are a few noteworthy comments for Figs. 2 and 3.

- The change from  $f_o > f$  below transition to  $f_o < f$  above transition is seen to happen automatically as expected with the cavity tuning control feedback
- The initial  $f_o < f$  at the beginning of the cycle can be either (1) an error in the  $f(I_{FBS})$  function, or (2) real due to the station ‘holding’ a slightly erroneous  $I_{FBS}$  value before beam is injected
- The incremental increase in the detuning as the 5 NuMI batches are injected is as expected due to the incremental increase in the average beam loading.

## Transfer Function Analysis Block Diagram

A transfer function block diagram of the cavity tuning control system is shown in Fig.4. It is the intent of this note to document the details of the various elements of this transfer function model to further the understanding of the present loop, to guide future upgrades, and to provide a mathematical model that can be included in RF system simulations and analysis.

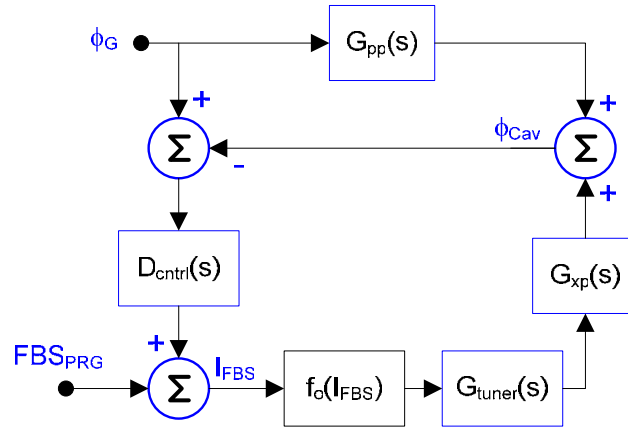


**Figure 4:** Simplified transfer function block diagram of the cavity tuning control system

The components of Fig.4 are:

- $f_o(I_{FBS})$  is not a transfer function, but rather describes the functional relationship between the cavity resonant frequency and the ferrite tuner biasing current as discussed above.
- $G_{tuner}(s)$  is the transfer function describing the response of the cavity resonant frequency to changes in the ferrite tuner biasing due to Eddy current effects.
- $G_{xp}(s)$  is the transfer function relating modulations of the cavity resonant frequency to modulations of the cavity voltage phase,  $\phi_{Cav}$ .
- $D_{ctrl}(s)$  is the transfer function for the cavity tuning controller feedback control function.
- $G_{pp}(s)$  is the transfer function relating modulations of the generator current phase,  $\phi_G$ , to modulations of  $\phi_{Cav}$ .

$G_{pp}(s)$  is not needed to characterize the closed loop response of the cavity tuning control loop. However, it is included in the diagram above to show where the tuning loop would fit into a larger system diagram. The dynamic measurements shown here effectively used a constant  $\phi_G$  such that  $G_{pp}(s)$  did not affect the measurements (i.e. upstream phase loops were opened)

The sections to follow describe the components of this model in detail:

## $f_o(I_{FBS})$ Curve Fitting:

Two possible curve fitting functions have been found for  $f_o(I_{FBS})$ :

- A 3<sup>rd</sup> order polynomial of the form:  $f_o(I_{FBS}) \cong c_0 + c_1 I_{FBS} + c_2 I_{FBS}^2 + c_3 I_{FBS}^3$
- An exponential function of the form:  $f_o(I_{FBS}) \cong k_0 \left(1 - e^{-k_1(I_{FBS}-k_2)}\right) + k_3$

where  $c_i$  and  $k_i$  are coefficients. The 3<sup>rd</sup> order polynomial function fits the original data with less error than the exponential function; however, it does not lend itself well to extrapolation since it is not monotonically increasing in domains used for extrapolation. The exponential function is monotonically increasing; thus preventing multiple closed loop stable points that could present errors in simulations.

An example curve fit for the MI-60 test station cavity S/N 17 is shown in Figs. 5 and 6.

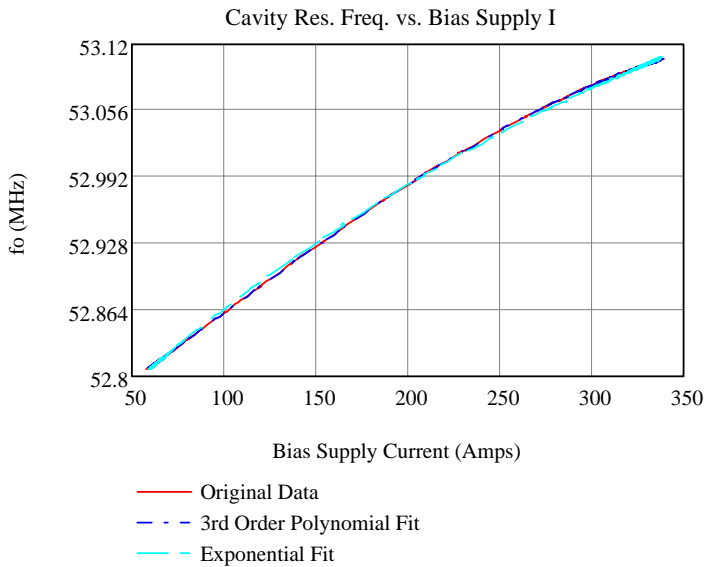


**Figure 5:** Example  $f_o(I_{FBS})$  curve fits for MI-60 test station cavity S/N 17.

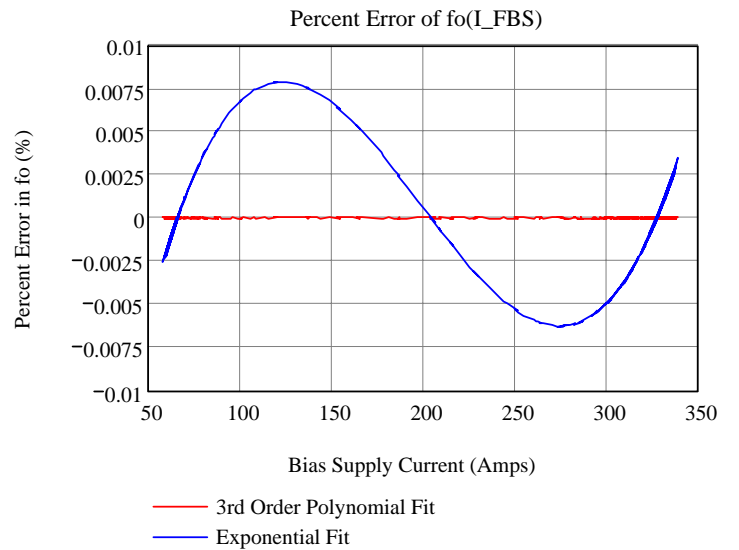


**Figure 6:** Percent error in  $f_o(I_{FBS})$  for Fig. 4.  
Note: 0.0075% corresponds to ~4 kHz.

The inverse function  $I_{FBS}(f_o)$  can find the required  $I_{FBS}$  for a desired  $f_o$ ; which would be useful for a ‘smart’ cavity tuning controller. Again, two possible curve fitting functions are:

- A 3<sup>rd</sup> order polynomial of the form:  $I_{FBS}(f_o) \cong C_0 + C_1 f_o + C_2 f_o^2 + C_3 f_o^3$
- A logarithmic function of the form:  $I_{FBS}(f_o) \cong k_2 - \frac{1}{k_1} \ln\left(1 - \frac{f_o - k_3}{k_0}\right)$

where  $C_i$  are coefficients that have to be found via a separate regression method than that for  $c_i$  and  $k_i$  are the same coefficients for the exponential  $f_o(I_{FBS})$  fit above.

Example fits for  $I_{FBS}(f_o)$  for the MI-60 test station cavity S/N 17 are shown in Figs. 7 and 8.

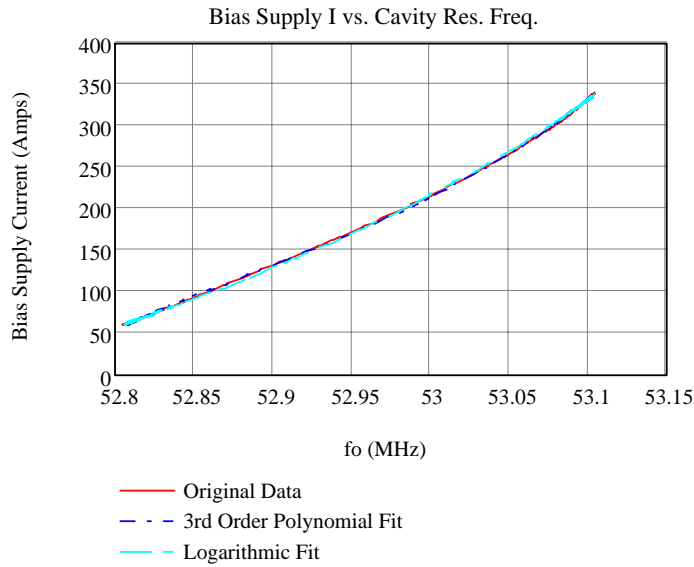


**Figure 7:** Example  $I_{FBS}(f_o)$  curve fits for MI-60 test station cavity S/N 17.

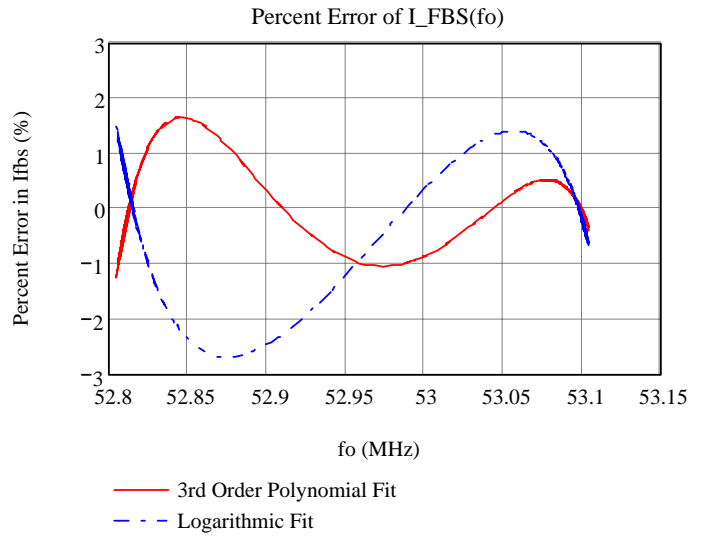


**Figure 8:** Percent error in  $I_{FBS}(f_o)$  for Fig. 4.

The curve fitting coefficients for all MI stations are given in Table I on the following page:

**Table 1:**  $f_o(I_{FBS})$  and  $I_{FBS}(f_o)$  Curve Fit Coefficients

Station	$f_o(I_{FBS})$ - Polynomial Fit Coefficients				$f_o(I_{FBS}), I_{FBS}(f_o)$ - Exp, Log Fit Coefficients				$I_{FBS}(f_o)$ - Polynomial Fit Coefficients			
	$c_0$	$c_1 [10^{-3}]$	$c_2 [10^{-6}]$	$c_3 [10^{-10}]$	$k_0$	$k_1 [10^{-3}]$	$k_2$	$k_3$	$C_0 [10^9]$	$C_1 [10^7]$	$C_2 [10^6]$	$C_3 [10^4]$
1	52.733	1.379	-1.063	-2.713	2.836	3.240	-524.766	50.401	-1.691	9.589	-1.813	1.143
2	52.738	1.349	-0.947	-4.331	2.846	3.163	-538.624	50.398	-1.612	9.142	-1.729	1.089
3	52.733	1.367	-1.463	4.712	2.803	3.184	-551.418	50.406	-1.962	11.130	-2.105	1.327
4	52.718	1.428	-0.605	-12.750	2.877	3.189	-503.488	50.399	-1.229	6.972	-1.318	0.831
5	52.729	1.284	-0.550	-9.037	2.856	2.982	-551.906	50.407	-1.532	8.688	-1.643	1.035
6	52.684	1.362	-1.359	4.716	2.782	2.854	-573.912	50.432	-1.903	10.795	-2.042	1.287
7	52.693	1.430	-1.581	6.360	2.786	3.067	-546.048	50.419	-1.838	10.431	-1.973	1.244
8	52.713	1.361	-1.328	3.431	2.798	3.051	-554.847	50.418	-1.895	10.753	-2.034	1.282
9	52.727	1.391	-0.985	-4.123	2.849	3.113	-533.287	50.406	-1.400	7.940	-1.502	0.946
10	52.703	1.324	-1.348	4.776	2.771	2.882	-583.555	50.439	-1.942	11.016	-2.084	1.314
11	52.708	1.269	-1.344	5.318	2.742	2.905	-595.382	50.444	-2.671	15.156	-2.866	1.807
12	52.726	1.228	-0.884	-1.045	2.797	2.867	-587.476	50.434	-1.932	10.961	-2.073	1.306
13	52.722	1.439	-1.500	3.822	2.802	3.306	-519.353	50.412	-1.809	10.264	-1.941	1.224
14	52.705	1.139	-1.002	3.016	2.741	2.542	-663.056	50.461	-2.545	14.440	-2.731	1.722
15	52.695	1.189	-1.130	3.978	2.731	2.643	-637.711	50.460	-2.793	15.845	-2.997	1.889
16	52.704	1.380	-1.075	-0.645	2.822	2.953	-546.455	50.428	-1.428	8.101	-1.532	0.966
17	52.669	1.391	-1.585	7.195	2.729	2.895	-574.345	50.451	-2.569	14.579	-2.758	1.739
18	52.687	1.317	-1.262	4.030	2.766	2.810	-583.622	50.445	-2.023	11.479	-2.171	1.369
Test Sta	52.727	1.306	0.491	-31.28	2.959	2.606	-564.011	50.429	-0.790	4.479	-0.850	0.534

Note:

- (1) The test station requires less  $I_{FBS}$  near extraction frequencies than the operational stations. This could possibly be due to temperature differences. The operational stations are run with a higher duty cycle than the test station was run at during the measurements.
- (2) A simple temperature effect measurement was made on Station 1 on a day when the MI RF was shut off for a few hours and then turned back on. Within fifteen minutes of turning on, the temperature rise of the cavities had changed  $f_o(I_{FBS})$  by as much as -12 kHz (the full 3dB bandwidth for a Q of 5000 @53.104 MHz is ~11 kHz) near extraction for the same  $I_{FBS}$ ; implying that the cavity resonant frequency increased due to thermal expansion and required a higher  $I_{FBS}$  to achieve the ~53.104 MHz extraction frequency.

## Dynamic Response of the Cavity Ferrite Tuners: $G_{\text{tuner}}(s)$

The cavity ferrite tuners are ferrite loaded coaxial inductive stubs that provide the effective variable inductance in the cavity circuit of Fig.1. The permeability of the ferrite material is adjusted via a biasing magnetic field which is generated via current loops that wrap around the inner and outer conductors of the coaxial stub. Eddy currents generated in the inner and outer conductors oppose changes in the biasing magnetic field; giving rise to a dynamic response to a change in the cavity resonant frequency.

A simple first order model of this dynamic response is represented by Fig.9a. The Ferrite Bias Supply is represented as an ideal current source  $I_{FBS}$ . The magnetic flux coupling between the magnetic bias windings and the eddy currents is represented as a transformer with coils of inductance  $L_{\text{tuner}}$  and  $L_{\text{Eddy}}$  with mutual inductance  $M = \sqrt{L_{\text{tuner}}L_{\text{Eddy}}}$ .  $R_{\text{tuner}}$  and  $R_{\text{Eddy}}$  represent the resistive losses associated with the tuner windings and eddy currents respectively. The biasing magnetic flux,  $\Phi$ , is assumed to be proportional to the difference of the currents  $I_{FBS}$  and  $I_{\text{Eddy}}$  in  $L_{\text{tuner}}$  and  $L_{\text{Eddy}}$  respectively ( $\Phi \propto I_{FBS} - I_{\text{Eddy}}$ ). Assuming the transformer is linear, the circuit of Fig.9a can be converted to that of Fig.9b. Additionally, for simplicity, if it is assumed that  $L_{\text{tuner}} = L_{\text{Eddy}}$  the circuit of Fig.9b further reduces to that of Fig. 9c. It is now clear that when  $I_{FBS}$  initially steps on,  $I_{\text{Eddy}}$  will equal  $I_{FBS}$ , thus making the initial biasing flux equal

to zero. Using the LaPlace variable  $s = j\omega$ ,  $I_{\text{Eddy}} = \frac{s}{s + (R_{\text{Eddy}} / M)} \cdot I_{FBS}$ . Thus, a first order

transfer function for the flux is  $\frac{\Phi}{I_{FBS}} \propto \left[ \frac{(R_{\text{Eddy}} / M)}{s + (R_{\text{Eddy}} / M)} \right] = \frac{p}{s + p}$ . This simple single pole model

can also be used to model the dynamic behavior of  $\Delta f$  (Eq.3) to a change in the FBS current if it is assumed that the cavity resonant frequency is proportional to the tuner's biasing flux.

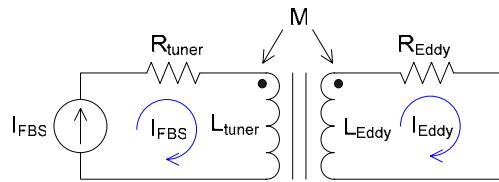


Fig. 9a

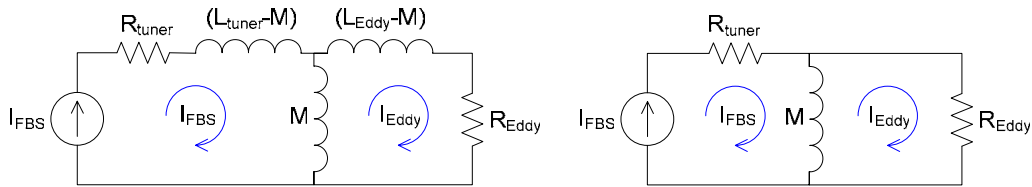


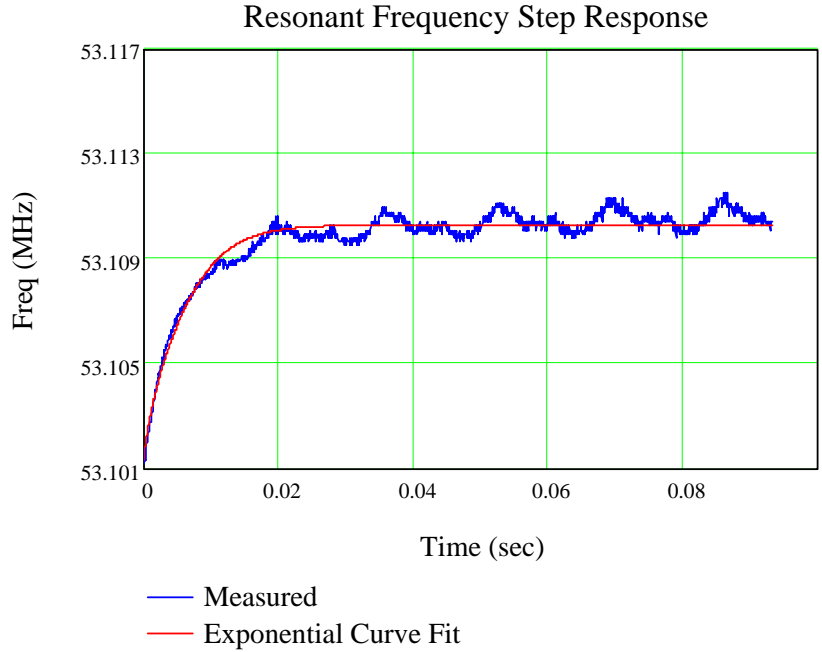
Fig. 9b

Fig. 9c

The value of this single pole was measured at the MI-60 test station. A step change in the FBS current was made while monitoring  $\phi_z$  with the anode-to-cathode phase detector. Assuming a linear change in the cavity Q from 3000 at the MI injection frequency (52.8114 MHz) to 5000 at the MI extraction frequency (53.104 MHz), Eq. 2 was used to determine the cavity resonant frequency  $f_o$  from  $\phi_z$ . An example measurement at an RF drive frequency of 53.104 MHz is shown in Fig. 10 along with a curve fit of the form

$$f_o(t) = f_{final} \left( 1 - e^{-\frac{t}{\tau}} \right) \text{ where } \tau$$

is the time constant of the dynamic response. The measured time constant was  $\sim 5.8$  msec; corresponding to a single pole,  $p$ , at  $\sim 27.4$  Hz for the model discussed above.



**Figure 10:** Example resonant frequency step response measurement.

### Cavity Response to Tuner Modulations $G_{xp}(s)$ :

Cavity resonant frequency or tuning variations change the cavity differential equations into time-varying equations. In general the tuning variations will cause additional amplitude and phase modulations of the cavity voltage. For small variations the phase modulations can be modeled as an additional linear transfer function  $G_{xp}(s)$  given by [1],

$$G_{xp}(s) = \frac{\sigma \cdot (s + \sigma)}{s^2 + 2\sigma s + \sigma^2 (1 + \tan^2 \phi_z)}$$

where  $\sigma = \frac{\pi f_o}{Q}$  is the damping rate parameter of the cavity impedance. This transfer function

has the same zero and poles as the un-normalized in-phase and quadrature modulation transfer functions as discussed in [2] as opposed to the normalized versions discussed in [1]. Note that for zero detuning,  $\phi_z = 0$ , the cavity response is a single pole at  $-\sigma$  corresponding to the half-bandwidth of the cavity impedance as expected. For a Q between 3000 and 5000, the corresponding pole is between  $\sim 5$ kHz to 9kHz.

It is now clear that, to first order, the composite cavity response to tuner modulations,  $G_{numer}(s) \cdot G_{xp}(s)$ , is effectively a second order system. A natural choice for a feedback controller is a conventional lead-lag compensator design; which was what was designed into the original controller as will be seen below.



The DC gain through the various paths to the FBS Drive output were measured to be:

- Program output:  $\sim FBS_{Pr_g} \cdot [0.45 + 0.045 \cdot DAC1 + 0.0045 \cdot DAC0]$
- Offset output:  $\sim [0.5 V + 0.04 \cdot DAC0]$
- Error output:  $\sim \phi_{error} [54 + 13 \cdot FBS_{Pr_g}]$

### $D_{ctrl}(s)$ Feedback Filter Response :

The feedback filter,  $D(s)$ , of Fig.11 is a lead-lag compensator op-amp circuit as shown in Fig.12.

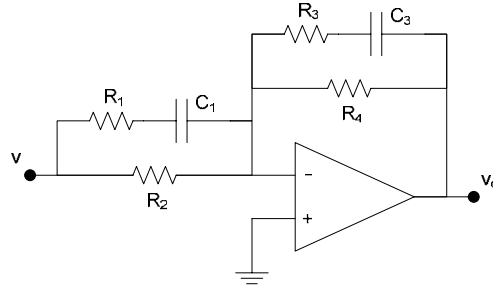


**Figure 12:** Lead-Lag op-amp circuit

The transfer function of the lead-lag circuit is:

$$D_{ctrl}(s) = \frac{v_o(s)}{v_i(s)} = \frac{R_3 R_4 (R_1 + R_2)}{R_1 R_2 (R_3 + R_4)} \cdot \frac{\left[ s + \frac{1}{R_3 C_3} \right]}{\left[ s + \frac{1}{C_3 (R_3 + R_4)} \right]} \cdot \frac{\left[ s + \frac{1}{C_1 (R_1 + R_2)} \right]}{\left[ s + \frac{1}{R_1 C_1} \right]} = K \cdot \frac{(s + z_1)}{(s + p_1)} \cdot \frac{(s + z_2)}{(s + p_2)}$$

where the first composite term is a gain term and the second and third terms are each either a lead or lag network depending upon the component values. The values used in the present cavity tuning controller are:  $R_1 = 120\Omega$ ,  $R_2 = 3k\Omega$ ,  $R_3 = 120\Omega$ ,  $R_4 = 100k\Omega$ ,  $C_1 = 0.033\mu F$ , and  $C_3 = 3.2\mu F$  resulting in the lag network of  $z_1 \cong 2\pi \cdot 414.5$ ,  $p_1 \cong 2\pi \cdot 0.5$  and the lead network of  $z_2 \cong 2\pi \cdot 1.55k$ ,  $p_2 \cong 2\pi \cdot 40.2k$  with gain  $K \cong 1.04$ . The DC gain of this circuit is  $R_4 / R_2 \cong 33$ . Note however, that the overall DC gain of the feedback through the cavity tuning controller is a function of the FBS program as described above. A bode plot of the compensator with these parameters is shown in Fig.13.

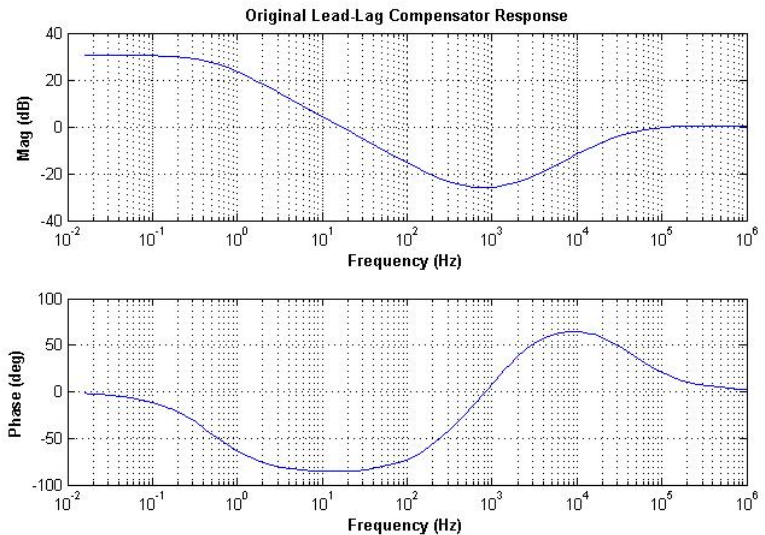


**Figure 13:** Original lead-lag compensator response

## Complete System Response

The approximate small signal open-loop response of the complete system,  $D_{ctrl}(s) \cdot G_{tuner}(s) \cdot G_{xp}(s)$ , at a DC gain of  $\sim 165$  is shown below in Fig.14.

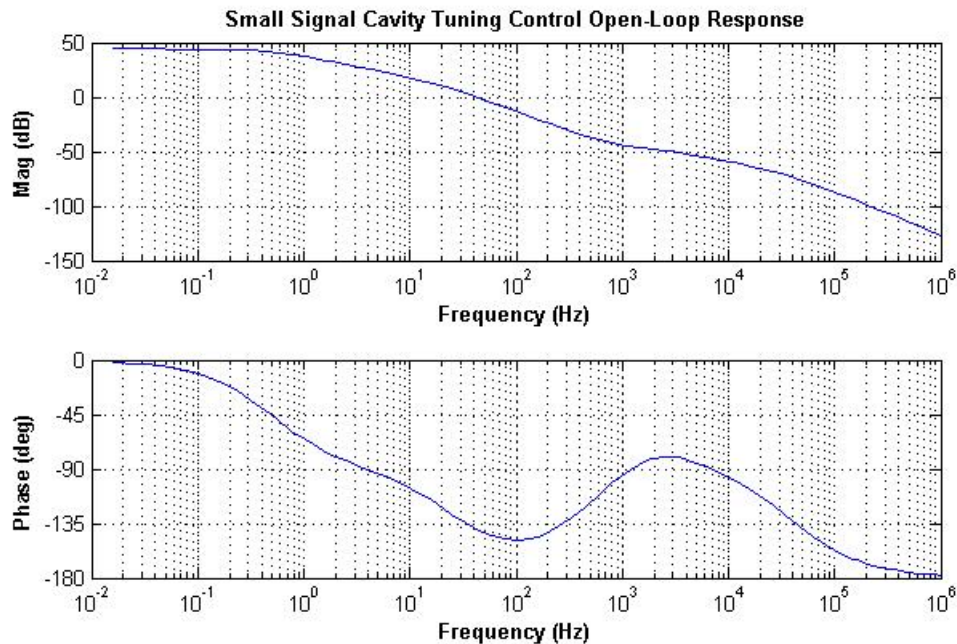


**Figure 14:** Approximate small signal open-loop response of the complete system,

Figure 15 below shows the measured amplitude and phase response of an actual station with the cavity tuning control loop active (closed-loop) along with a simulation. The measurement was taken at the MI-60 test station with the cavity initially detuned by  $\sim 70$ deg when the cavity tuning control loop was initially activated. The saturation seen at the peaks of the amplitude is due to the power amplifier tube drawing screen current and entering saturation.

The simulation was performed using Simulink<sup>1</sup>. The Simulink model includes the full time-varying state-space model for the cavity based upon the in-phase and quadrature transfer functions for a resonant cavity from Ref. [2]. The exponential fit for  $f_o(I_{FBS})$  and the single pole model for  $G_{tuner}(s)$  was used to model the test station cavity ferrite tuners. The simulation gain had to be  $\sim 3$  times higher than the small signal gain shown in Fig.14 to achieve similar results. This is possibly due to higher frequency poles and parasitic poles reducing the phase margin of the system. Further investigations would be necessary to completely understand the gain difference. Overall, the comparison places confidence in the simulation model at least to first order.

<sup>1</sup> Simulink is software for modeling, simulating, and analyzing dynamic systems. For more info see [www.mathworks.com](http://www.mathworks.com)

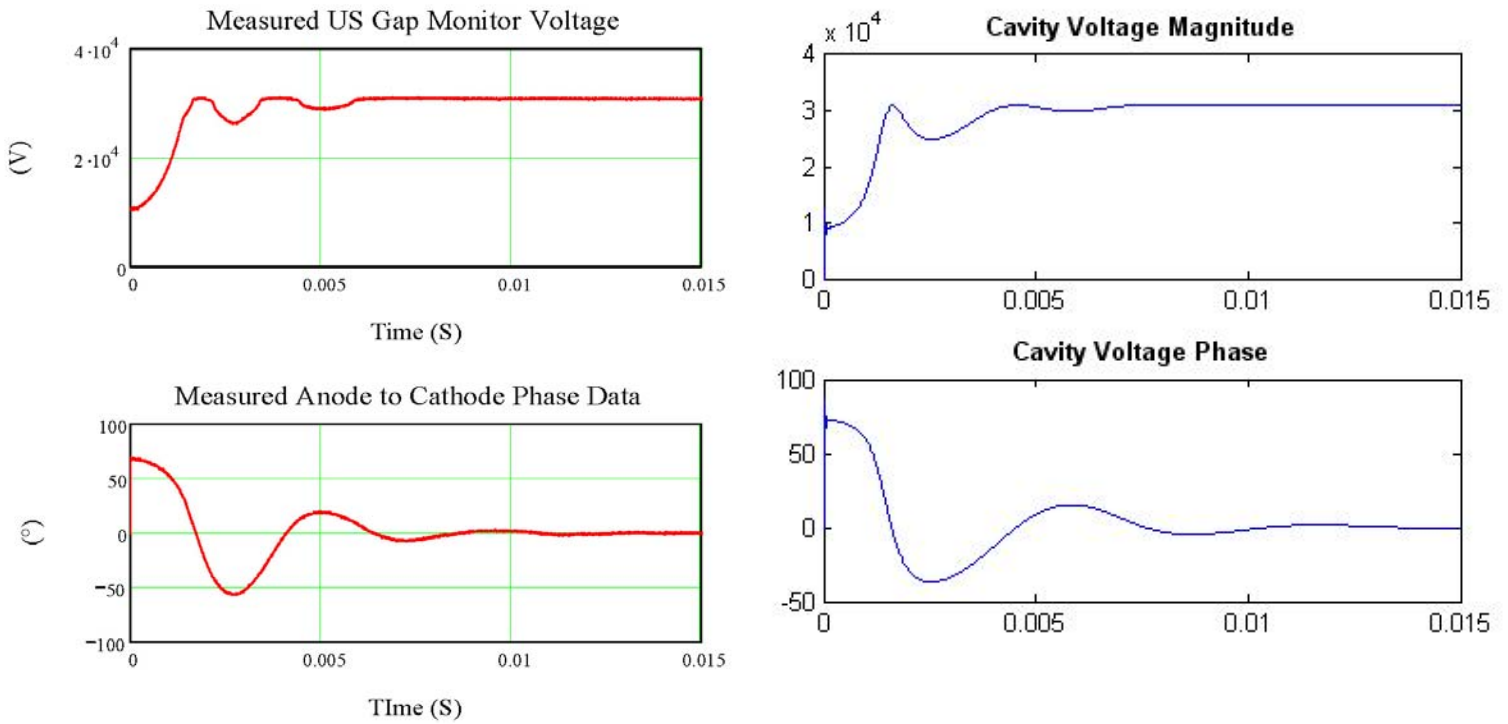


**Figure 15:** (Left) MI-60 test station measurement of cavity tuning control loop. (Right) Simulink simulation.

Looking back at Figs.13 and 14, it appears that the original design's intent was to increase the phase margin near the cavity pole with the lead compensator and to decrease the steady state error with an increased DC gain due to the lag compensator as expected. However, when looking at the Fig.14, it appears that increased phase margin might be obtained if the lead compensator's pole and zero were shifted to a slightly lower frequency. As a proof of principle that other tunings are possible, the lead compensator's pole and zero were scaled by a factor of 1/10 and the DC gain was increased by a factor of 7 to achieve a lower overshoot in simulations as shown in Fig.16.

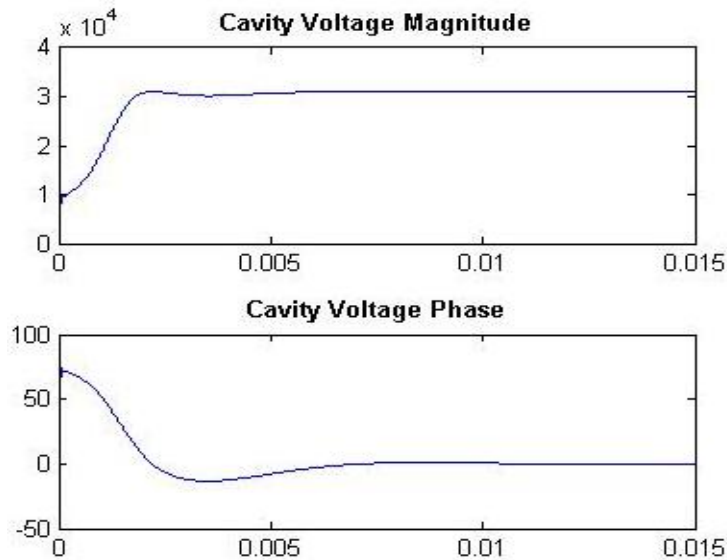


**Figure 16:** Simulink simulation with lead compensator's pole and zero at 1/10 the original values and DC gain 7 times the original. Horizontal axis is time, vertical is magnitude is Volts, vertical phase is Degrees.

## Conclusion

The original cavity tuning control system has been characterized to guide future upgrade designs. There are various methods available to tune the system response; including root locus methods, frequency response methods, and state-space methods. Modern tools are available that offer computational power that can be used to help optimize future designs. The model provided here has been included in a time-varying state space simulation of the cavity impedance. It can be included in full system simulations to help understand the coupling between the various RF system control loops; something which may become necessary as more loops are added to the system and cross-coupling between loops occur due to machine conditions.

## References

- [1] F.Pedersen, "Beam Loading Effects in the CERN PS Booster", IEEE Transactions on Nuclear Science, Vol NS-22, No.3, June 1975, pp 1906-1909.
- [2] T.Berenc, "IQ Modulation Transfer Functions for a Resonant Cavity", Fermilab RF TechNote #079, May 2006, <http://www-rfes.fnal.gov/global/technotes/TN/TN079.pdf>
- [3] D.Boussard, "Beam Loading", Sec. 2.5.2 of "Handbook of Accelerator Physics and Engineering" by Chao and Tigner, pp.108-112.
- [4] K.W. Robinson, CEA, Report No. CEAL-1010, Feb. 1964.
- [5] T.Berenc, "Main Injector HLRF Measurements for Proton Plan", Fermilab beams-doc#2331 July 2006.
- [6] Norman S. Nise, "Control Systems Engineering, Third Edition", John Wiley & Sons Inc., New York, 2000.